J. Fluid Mech. (1979), *vol.* 94, *part* 4, *pp.* 609–627
Printed in Great Britain

Nonlinear properties of convection rolls in a horizontal layer rotating about a vertical axis

By R. M. CLEVER AND F. H. BUSSE

Institute of Geophysics and Planetary Physics,
University of California, Los Angeles 90024

(Received 29 June 1978 and in revised form 25 January 1979)

Steady finite amplitude two-dimensional solutions are obtained for the problem of convection in a horizontal fluid layer heated from below and rotating about its vertical axis. Rigid boundaries with prescribed constant temperatures are assumed and the solutions are obtained numerically by the Galerkin method. The existence of steady subcritical finite amplitude solutions is demonstrated for Prandtl numbers $P < 1$. A stability analysis of the finite amplitude solutions is performed by superimposing arbitrary three-dimensional disturbances. A strong reduction in the domain of stable rolls occurs as the rotation rate is increased. The reduction is most pronounced at low Prandtl numbers. The numerical analysis confirms the small amplitude results of Küppers & Lortz (1969) that all two-dimensional solutions become unstable when the dimensionless rotation rate Ω exceeds a value of about 27 at $P \simeq \infty$. A brief discussion is given of the three-dimensional time-dependent forms of convection which are realized at rotation rates exceeding the critical value.

1. Introduction

The calculation of finite amplitude convection in a layer heated from below has become a favoured problem of numerical computation in fluid mechanics ever since the first high-speed electronic computers became available. The steady two-dimensional solution of the basic equations represents a physically realistic form of convection for a fairly wide range of parameters in contrast to other problems of hydrodynamic instability which, in general, are time dependent and lead to a three-dimensional form of turbulence. That two-dimensional numerical solutions of convection can be readily obtained must not detract from the fact that various forms of three-dimensional convection are often realized, especially at higher Rayleigh numbers. Since three-dimensional numerical computations are still too expensive as a routine method for the analysis of convection, the much less expensive analysis of the stability of two-dimensional convection with respect to three-dimensional disturbances is of particular importance.

In rotating as well as non-rotating convection layers, steady two-dimensional rolls represent the preferred form of convection at Rayleigh numbers close to the critical value according to the small amplitude theories of Schlüter, Lortz & Busse (1965) and Küppers & Lortz (1969). The familiar hexagonal cells appear only if deviations from the Boussinesq approximation are taken into account (see, for example, Busse, 1967*a*) which will not be considered in this paper. The transition to three-dimensional

0022–1120/79/4281–7460 $02.00

forms of convection at higher Rayleigh numbers occurs in general in the form of an instability with disturbances growing from infinitesimal amplitudes. Thus the spatial structure of the three-dimensional form of convection can usually be inferred from the form of the strongest-growing disturbance determined by the linear stability analysis of the stationary convection rolls. In addition, the oscillatory or monotonic time dependence of the disturbance determines the nature of the time dependence of the ultimately realized three-dimensional form of convection.

The close correspondence between the strongest growing disturbances and the experimentally realized form of three-dimensional convection has first been demonstrated in the case of bimodal convection (Busse & Whitehead 1971). The laboratory observations confirmed essentially all aspects of the earlier stability analysis of Busse (1967*b*). Since then a similarly close correspondence between theoretical results and experimental observations has been found in the case of oscillatory convection (Busse 1972; Clever & Busse 1974) and in the cases of the knot instability (Busse & Clever 1979*a*) and the wavy instability of convection rolls in an inclined layer (Hart 1971; Clever & Busse 1977).

The present paper is a sequel to those mentioned in that the analysis by Clever & Busse (1974) of instabilities of convection rolls in a horizontal layer is extended to the case when the layer is rotating about a vertical axis. The stability analysis for a rotating system is of special interest because three-dimensional forms of convection appear to be more predominant than in a non-rotating system and the nature of the three-dimensional convection patterns observed in experiments has not yet been clearly understood. In the three major experimental studies of convection in a rotating system that have been published in the literature (Rossby 1969; Koschmieder 1967; Krishnamurti 1971), a transition from two-dimensional roll-like convection to three-dimensional cellular convection was observed and attributed to a variety of causes, for instance, the effect of the circulation induced by the centrifugal force or the instability found by Küppers & Lortz (1969). Because little quantitative data were obtained, it is difficult to separate different mechanisms. One of the goals of the comprehensive stability analysis given in this paper is to provide a framework for the interpretation of future experimental observations.

The instability discovered by Küppers & Lortz (1969) is one of the most interesting phenomena of hydrodynamic stability theory. For low values of the Taylor number Küppers & Lortz found in agreement with the results of Schlüter *et al.* (1965) in the non-rotating case that, among all possible three-dimensional patterns of convection, only convection in the form of two-dimensional rolls represents a stable solution of the basic equations near the critical value of the Rayleigh number. But, for Taylor numbers T exceeding the critical value $T_c = 2285$, convection rolls become unstable and no stable stationary solution for convection is available. Since oscillatory motions are precluded in the limit of infinite Prandtl number which was assumed by Küppers & Lortz, the question of the physically realized convection flow represents an enigmatic problem. A recent study of the problem has reached the conclusion that the realized form of convection in the presence of the Küppers–Lortz instability is governed by the level of experimental noise (Busse & Clever 1978*b*).

The original work of Küppers & Lortz, who had assumed stress-free boundary conditions, has been extended by Küppers (1970) to the case of finite Prandtl numbers and rigid boundaries. Except for variations of the value of T_c with the Prandtl

number, the results remained essentially unchanged. For the comparison with experiments, it seems necessary to analyse the Küppers–Lortz instability for Rayleigh numbers outside the neighbourhood of the critical value since observations at low amplitudes of convection are difficult to make. The present paper accomplishes this task. Although the method of analysis is quite different from that used by Küppers (1970), the results agree well in the common domain of validity at small convection amplitudes.

The paper starts with the formulation of the basic equation and an outline of the numerical analysis for the case of the steady solution, as well as for the subsequent stability investigation with respect to arbitrary three-dimensional disturbances. In most respects the analysis follows that of Busse (1967*b*) and Clever & Busse (1974). The latter paper will be referred to as CB. The numerical results for steady two-dimensional convection are discussed in § 3. The results of the stability analysis described in § 4 represent by far the major part of the computational effort. A general discussion and some more speculative thoughts are given in § 5.

2. Mathematical formulation of the problem

2.1. *Basic equations*

We consider a horizontal layer of fluid contained between two rigid, perfectly conducting boundaries separated by the distance d. The constant temperatures T_1 and T_2 are prescribed at the upper and lower boundaries. The layer is rotating about a vertical axis with the rate Ω_D. We assume that the centrifugal force is negligible in comparison with gravity. Thus the problem retains the properties of isotropy and homogeneity with respect to the horizontal dimensions of the non-rotating case. The analysis is based on the Boussinesq approximation of the equations of motion and the heat conduction equation. Using d, d^2/κ and $(T_2-T_1)/R$ as scales for length, time and temperature, respectively, the dimensionless equations for the velocity vector $\mathbf{v}$ and the deviation θ of the temperature from the static distribution can be written in the form

$$\nabla^2\mathbf{v}+\boldsymbol{\lambda}\theta-\nabla\Gamma-2\Omega\boldsymbol{\lambda}\times\mathbf{v}=P^{-1}\left(\mathbf{v}.\nabla\mathbf{v}+\frac{\partial}{\partial t}\mathbf{v}\right), \tag{2.1a}$$

$$\nabla.\mathbf{v}=0 \tag{2.1b}$$

and

$$\nabla^2\theta+R\boldsymbol{\lambda}.\mathbf{v}=\mathbf{v}.\nabla\theta+\frac{\partial}{\partial t}\theta. \tag{2.1c}$$

The physical parameters of the problem are expressed in terms of three dimensionless numbers

$$R=\gamma g(T_2-T_1)\,d^3/\kappa\nu,\quad \Omega=\Omega_D d^2/\nu \quad\text{and}\quad P=\nu/\kappa,$$

called the Rayleigh number, rotation parameter, and Prandtl number, respectively; ν is the kinematic viscosity, κ is the thermal diffusivity, γ is the coefficient of thermal expansion and g is the acceleration of gravity. The unit vector $\boldsymbol{\lambda}$ is directed opposite to gravity and $\nabla\Gamma$ includes all terms that can be written in the form of a gradient.

In order to eliminate the equation of continuity (2.1*b*) from the problem, the following general representation for a solenoidal vector field is introduced:

$$\mathbf{v}=\boldsymbol{\delta}\phi+\boldsymbol{\epsilon}\psi,$$

where the operators $\boldsymbol{\delta}$ and $\boldsymbol{\epsilon}$ are defined by

$$\boldsymbol{\delta}\phi \equiv \nabla \times (\nabla \times \boldsymbol{\lambda}\phi) \quad \text{and} \quad \boldsymbol{\epsilon}\psi \equiv \nabla \times \boldsymbol{\lambda}\psi.$$

By operating with $\boldsymbol{\lambda}.\nabla\times(\nabla\times$ and $\boldsymbol{\lambda}.\nabla\times$ on equation (2.1a) and by rewriting equation (2.1c), the following system of three equations for the unknown scalar fields ϕ, ψ, and θ is obtained:

$$\nabla^4\Delta_2\phi - \Delta_2\theta - 2\Omega\partial_z\Delta_2\psi = P^{-1}\left\{\boldsymbol{\delta}.[(\boldsymbol{\delta}\phi+\boldsymbol{\epsilon}\psi).\nabla(\boldsymbol{\delta}\phi+\boldsymbol{\epsilon}\psi)] + \frac{\partial}{\partial t}\nabla^2\Delta_2\phi\right\}; \quad (2.2a)$$

$$\nabla^2\Delta_2\psi + 2\Omega\partial_z\Delta_2\phi = P^{-1}\left\{\boldsymbol{\epsilon}.[(\boldsymbol{\delta}\phi+\boldsymbol{\epsilon}\psi).\nabla(\boldsymbol{\delta}\phi+\boldsymbol{\epsilon}\psi)] + \frac{\partial}{\partial t}\Delta_2\psi\right\}; \quad (2.2b)$$

$$\nabla^2\theta - R\Delta_2\phi = (\boldsymbol{\delta}\phi+\boldsymbol{\epsilon}\psi).\nabla\theta + \frac{\partial}{\partial t}\theta; \quad (2.2c)$$

where $\partial_z\phi$ denotes the partial derivative of ϕ with respect to the z co-ordinate in the direction of $\boldsymbol{\lambda}$ and Δ_2 is the Laplacian with respect to the horizontal co-ordinates x and y.

Assuming the origin of the Cartesian system of co-ordinates in the centre of the layer, the conditions at the rigid boundaries can be expressed in the form

$$\phi = \partial_z\phi = \psi = \theta = 0 \quad \text{at} \quad z = \pm\tfrac{1}{2}. \quad (2.3)$$

The problem defined by equations (2.2) and boundary conditions (2.3) is considered in two special cases. First, steady two-dimensional solutions will be obtained as a function of R, Ω, P, and the horizontal wavenumber α. In a second step, equations (2.2) will be solved for arbitrary infinitesimal three-dimensional disturbances superimposed onto the steady solution. The domain in the parameter space for which all possible disturbances decay represents the region of physically realizable convection rolls.

2.2. *The steady problem*

Assuming that the variables ϕ, ψ, and θ depend only on the y and z co-ordinates, equations (2.2) can be written in the form

$$\partial_y(\nabla^4\phi - \theta - 2\Omega\partial_z\psi) = P^{-1}\{\partial^2_{yz}\phi\,\partial^4_{yyzz}\phi - \partial^2_{yy}\phi\,\partial^4_{yzzz}\phi + \partial^2_{yz}\phi\,\partial^4_{yyyy}\phi - \partial^2_{yy}\phi\,\partial^4_{yyyz}\phi\} \quad (2.4a)$$

and

$$\partial_y(\nabla^2\psi + 2\Omega\partial_z\phi) = P^{-1}\{\partial^2_{yz}\phi\,\partial^2_{yy}\psi - \partial^2_{yy}\phi\,\partial^2_{yz}\psi\}, \quad (2.4b)$$

$$\nabla^2\theta - R\,\partial^2_{yy}\phi = \partial^2_{yz}\phi\,\partial_y\theta - \partial^2_{yy}\phi\,\partial_z\theta. \quad (2.4c)$$

These equations are solved numerically by using a Galerkin technique. Accordingly, ϕ, ψ, and θ are expanded in terms of orthogonal functions that satisfy the respective boundary conditions:

$$\phi = \sum_{\lambda\nu} a_{\lambda\nu} e^{i\lambda\alpha y} g_\nu(z) \equiv \sum_{\lambda\nu} a_{\nu\lambda}\phi_{\lambda\nu}; \quad (2.5a)$$

$$\psi = \sum_{\lambda\nu} c_{\lambda\nu} e^{i\lambda\alpha y} f_\nu(z) \equiv \sum_{\lambda\nu} c_{\lambda\nu}\psi_{\lambda\nu}; \quad (2.5b)$$

$$\theta = \sum_{\lambda\nu} b_{\lambda\nu} e^{i\lambda\alpha y} f_\nu(z) \equiv \sum_{\lambda\nu} b_{\lambda\nu}\theta_{\lambda\nu}; \quad (2.5c)$$

where the summation runs through all integers $-\infty < \lambda < \infty$, $1 \leqslant \nu < \infty$. The functions $f_\nu(z)$ represent $\sin[\nu\pi(z+\frac{1}{2})]$ and the functions $g_\nu(z)$ are given in Chandrasekhar's book (1961, p. 635) and are used in the same notation as in CB.

In order to compute the coefficients $a_{\lambda\nu}$, $b_{\lambda\nu}$, $c_{\lambda\nu}$ it is necessary to truncate the representations (2.5) at a sufficiently high level. As in the earlier work we choose the

truncation parameters N such that all coefficients with $|\lambda|+\nu > N$ are neglected. After substituting expansions (2.5) into (2.4), multiplying them by $\phi_{\kappa\mu}$, $\psi_{\kappa\mu}$, and $\theta_{\kappa\mu}$, respectively, and averaging over the fluid layer a system of nonlinear algebraic equations is obtained for the unknowns $a_{\lambda\nu}$, $b_{\lambda\nu}$, $c_{\lambda\nu}$ analogous to system (13) of CB. Because of the symmetry of the basic equations it is sufficient to restrict the analysis to solutions that are symmetric in y and satisfy

$$a_{\lambda\nu} = a_{-\lambda\nu}, \quad b_{\lambda\nu} = b_{-\lambda\nu} \quad \text{and} \quad c_{\lambda\nu} = c_{-\lambda\nu}. \tag{2.6}$$

The computational effect can be reduced further by realizing that equations (2.4) admit a subset of solutions with the property

$$\left.\begin{aligned} &\phi(z,y) = -\phi(-z,\pi/\alpha-y), \quad \theta(z,y) = -\theta(-z,\pi/\alpha-y),\\ &\psi(z,y) = \psi(-z,\pi/\alpha-y), \end{aligned}\right\} \tag{2.7}$$

which implies that the coefficients $a_{\lambda\nu}$ and $b_{\lambda\nu}$ vanish for odd values of $\lambda+\nu$ and the coefficients $c_{\lambda\nu}$ vanish for even values of $\lambda+\nu$. We shall restrict the attention to this subset of solutions, which includes the solutions realized close to the critical value of the Rayleigh number. Solutions of (2.4) that do not satisfy properties (2.7) such as the solutions describing a double layer of convection rolls exist only at much higher values of the Rayleigh number than those of interest in this paper and are generally not of physical interest.

Since the coefficients $a_{0\nu}$ and $c_{0\nu}$ do not appear in (2.4) they can be neglected and the total number of unknown coefficients becomes $\frac{3}{4}N^2$ for a given even value of the truncation parameter N. The $\frac{3}{4}N^2$ nonlinear algebraic equations are solved by a Newton–Raphson procedure. If reasonably close initial values are used, usually a solution for a lower value of the Rayleigh number, 5–10 iterates are sufficient to obtain a converged solution. As in CB, the truncation parameter N is chosen sufficently high such that the heat transport appears to approach within 1 % of its asymptotic value for $N\to\infty$. Because of the high derivatives involved in the heat transport, this criterion is especially sensitive to the convergence of the solution and has been found very satisfactory in the non-rotating case. According to the criterion, $N = 10$ is required to obtain a good approximation in the case of the highest Rayleigh numbers considered and also in the low Prandtl number cases mentioned in § 3.

2.3. *The stability analysis*

The equations for the field $\{\tilde\phi,\tilde\psi,\tilde\theta\}$ of infinitesimal disturbances is obtained by replacing ϕ, ψ, and θ in (2.2) by $\phi+\tilde\phi$, $\psi+\tilde\psi$, and $\theta+\tilde\theta$, respectively, and subtracting the equations for the steady solution $\{\phi,\psi,\theta\}$:

$$\begin{aligned}\nabla^4\Delta_2\tilde\phi - \Delta_2\tilde\theta - 2\Omega\,\partial_z\Delta_2\tilde\psi = P^{-1}\Big\{&\boldsymbol{\delta}\,.\,[(\boldsymbol{\delta}\tilde\phi+\boldsymbol{\epsilon}\tilde\psi)\,.\,\nabla(\boldsymbol{\delta}\phi+\boldsymbol{\epsilon}\psi)\\ &+(\boldsymbol{\delta}\phi+\boldsymbol{\epsilon}\psi)\,.\,\nabla(\boldsymbol{\delta}\tilde\phi+\boldsymbol{\epsilon}\tilde\psi)]+\frac{\partial}{\partial t}\nabla^2\Delta_2\tilde\phi\Big\}; \end{aligned} \tag{2.8a}$$

$$\begin{aligned}\nabla^2\Delta_2\tilde\psi + 2\Omega\,\partial_z\Delta_2\tilde\phi = P^{-1}\Big\{&\boldsymbol{\epsilon}\,.\,[(\boldsymbol{\delta}\tilde\phi+\boldsymbol{\epsilon}\tilde\psi)\,.\,\nabla(\boldsymbol{\delta}\phi+\boldsymbol{\epsilon}\psi)\\ &+(\boldsymbol{\delta}\phi+\boldsymbol{\epsilon}\psi)\,.\,\nabla(\boldsymbol{\delta}\tilde\phi+\boldsymbol{\epsilon}\tilde\psi)]+\frac{\partial}{\partial t}\Delta_2\tilde\psi\Big\}; \end{aligned} \tag{2.8b}$$

$$\nabla^2\tilde\theta - R\Delta_2\tilde\phi = (\boldsymbol{\delta}\tilde\phi+\boldsymbol{\epsilon}\tilde\psi)\,.\,\nabla\theta + (\boldsymbol{\delta}\phi+\boldsymbol{\epsilon}\psi)\,.\,\nabla\tilde\theta + \frac{\partial}{\partial t}\tilde\theta. \tag{2.8c}$$

Since the equations (2.8) do not exhibit an explicit dependence on x and t and since the y-dependence is periodic, the general solution of the stability problem can be obtained as a sum of solutions which depend exponentially on x and t, and which have a y-dependence with the same period as the steady solution multiplied by a factor $\exp\{idy\}$ called the Floquet factor in the corresponding problem for ordinary differential equations:

$$\tilde{\phi} = (\sum_{\lambda,\nu} \tilde{a}_{\lambda\nu} e^{i\lambda\alpha y} g_\nu(z)] \exp\{i(dy+bx)+\sigma t\}; \tag{2.9a}$$

$$\tilde{\psi} = (\sum_{\lambda,\nu} \tilde{c}_{\lambda\nu} e^{i\lambda\alpha y} f_\nu(z)) \exp\{i(dy+bx)+\sigma t\}; \tag{2.9b}$$

$$\tilde{\theta} = (\sum_{\lambda,\nu} \tilde{b}_{\lambda\nu} e^{i\lambda\alpha y} f_\nu(z)) \exp\{i(dy+bx)+\sigma t\}. \tag{2.9c}$$

Since $\tilde{\phi}, \tilde{\psi}$, and $\tilde{\theta}$ satisfy the same boundary conditions as ϕ, ψ, and θ, respectively, the same expansion functions have been used for the z-dependence. As in the case of the steady problem, a system of algebraic equations is obtained by multiplying (2.8a) by $\phi_{\kappa\mu}\exp\{-i(dy+bx)-\sigma t\}$, averaging it over the fluid layer and doing the analogous operations in the cases of (2.8b) and (2.8c). The resulting linear homogeneous equations represent an eigenvalue problem with the eigenvalue σ. Since the equations differ only by the addition of a few terms from equations (16) of CB, they are not given here explicitly.

Because of the symmetry of the steady solution, the equations for the coefficients $\tilde{a}_{\kappa\mu}, \tilde{b}_{\kappa\mu}$ with even $\kappa+\mu$ and the equations for the coefficients $\tilde{c}_{\kappa\mu}$ with odd $\kappa+\mu$ separate from the equations for which $\kappa+\mu$ has the opposite parity. Accordingly, instabilities with even $\kappa+\mu$ will be distinguished from those with odd $\kappa+\mu$ based on the symmetry of the coefficients $\tilde{a}_{\kappa\mu}$ and $\tilde{b}_{\kappa\mu}$. The same truncation parameter N is used for the disturbance representation (2.9) as for the steady solution.

To determine the domain of stability of the steady solution in the four-dimensional R, P, Ω, α space, the Rayleigh number is normally varied in small steps and the eigenvalue σ with largest real part is computed at each step as a function of b and d. The Rayleigh number at which the real part of this eigenvalue vanishes indicates the stability boundary. Usually the eigenvalues σ depend smoothly on the parameters of the problem and accurate results can be obtained by interpolation from a fairly coarse grid of computed eigenvalues σ.

3. The steady solution

Most of the numerical computations of two-dimensional convection published in the literature have been carried out without consideration of the stability of the solution. Thus in many cases solutions have been obtained for values of the parameters for which the two-dimensional solution is physically not realizable. This is particularly true in the case of a rotating layer, in which case the stability domain of convection rolls is much smaller than in the non-rotating case as the results of § 4 demonstrate. However, the computations of two-dimensional solutions are of interest beyond the range of stability of convection rolls, since they appear to exhibit some typical nonlinear properties of convection which experience little change when a transition to three-dimensional convection takes place. For example, the computed heat transport of two-dimensional convection in a non-rotating layer seems to

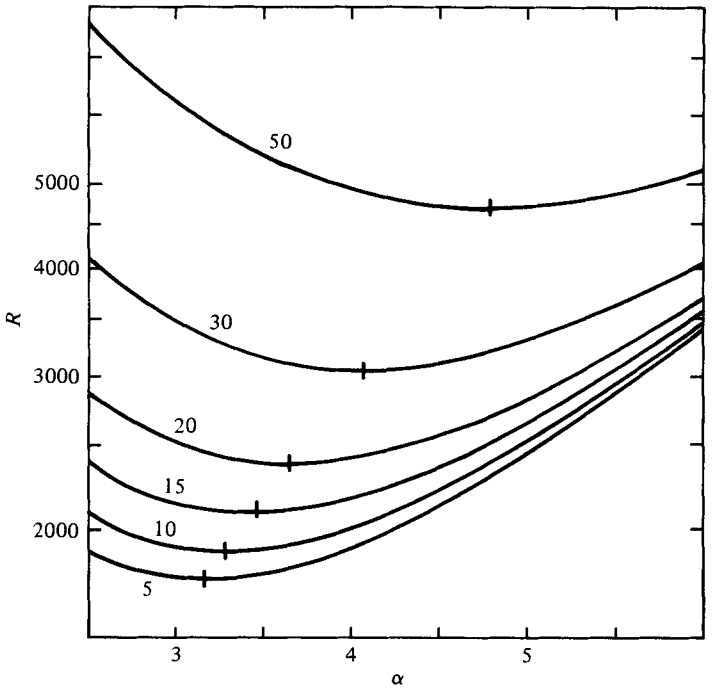

FIGURE 1. The critical Rayleigh number R_c for the onset of steady convection as a function of the wavenumber α. The curves correspond (from top to bottom) to Ω = 50, 30, 20, 15, 10, 5.

agree reasonably well with the observed values of turbulent convection, although it is not clear whether this indicates a general property of convection or whether it is due to an accidental compensation between the effects of three-dimensionality and time dependence.

As will be shown later, the Küppers–Lortz instability is the primary cause of the restricted stability domain of two-dimensional convection in a rotating system. This instability seems to have only a slight effect on the heat transport and we have computed for this reason the heat transport for values of Ω beyond the critical values of the Küppers–Lortz instability. Wherever possible, agreement has been found with the more restricted previous calculations of Somerville (1971). In all qualitative aspects the results also agree with those obtained by Veronis (1966, 1968) in the case of stress-free boundaries.

The heat transport is usually shown in terms of the Nusselt number which describes the ratio between the heat transport with convection and what it would be without convection at a given Rayleigh number. The curves seem to show a minimum of variation when plotted against $R - R_c$, where $R_c(\alpha, \Omega)$ represents the critical value of the Rayleigh number for the onset of convection in the form of infinitesimal steady motions. In figure 1 the function $R_c(\alpha, \Omega)$ is plotted for various values of Ω in order to facilitate the use of the Nusselt number graphs. Since few results for the onset of oscillatory convection in the presence of rigid boundaries are available in the literature, the critical value $R_0(\Omega)$ for the oscillatory mode is given in figure 2. The corresponding wavenumbers α_0 and frequencies σ_i of the oscillatory mode are given in figures 3 and 4, respectively.

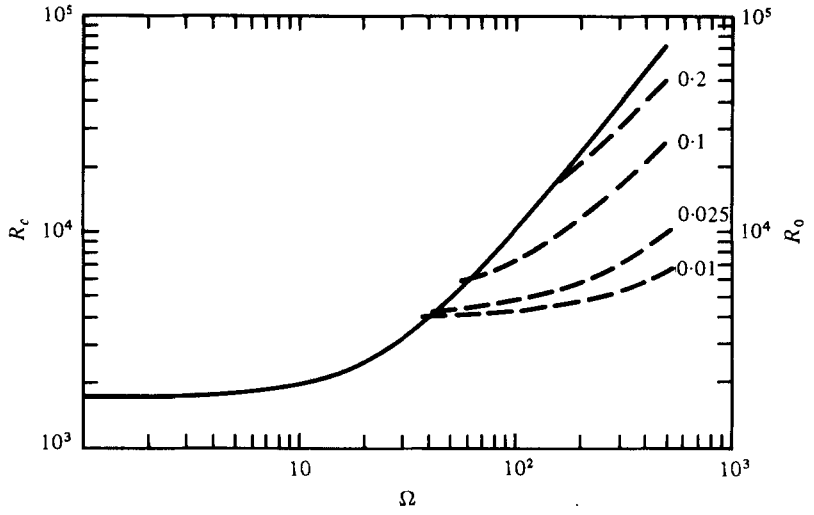

FIGURE 2. The critical Rayleigh number $R_c(\alpha_c)$ as a function of Ω for steady convection (solid curve). The critical Rayleigh number R_0 for the onset of oscillatory convection for four different Prandtl numbers is given by the dashed curves. The value of R_c for steady convection is independent of P.

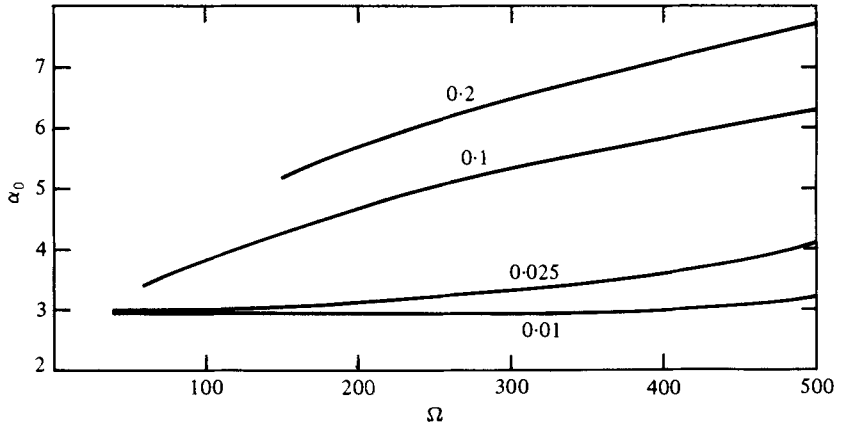

FIGURE 3. The critical wavenumber of oscillatory convection as a function of Ω for four different Prandtl numbers.

The Coriolis force appears to have a constraining effect on steady convection beyond the well-known delay of the onset of convection which is evident in figures 1 and 2. The results given in figure 5 indicate a noticeable decrease of the heat transport for large values of Ω, at least for $R - R_c$ less than 5×10^4. Beyond that value the Coriolis force enhances the heat transport at a given value of $R - R_c$. This effect is clearly evident in figure 6 where a typical rotating case is compared with the non-rotating results. There is no indication, however, that the heat transport in a rotating layer ever exceeds the heat transport in the non-rotating layer at given value of R in the case $P > 1$. The experimental results of Rossby (1969) which show just this effect in water must be either caused by some three-dimensional effect or by a change in

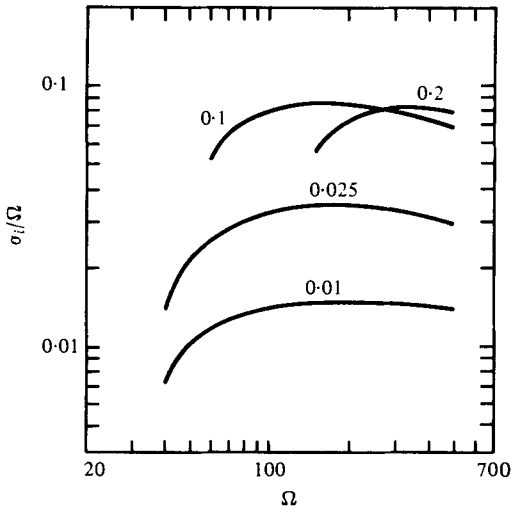

FIGURE 4. The frequency σ_i of oscillatory convection as a function of Ω for four different Prandtl numbers.

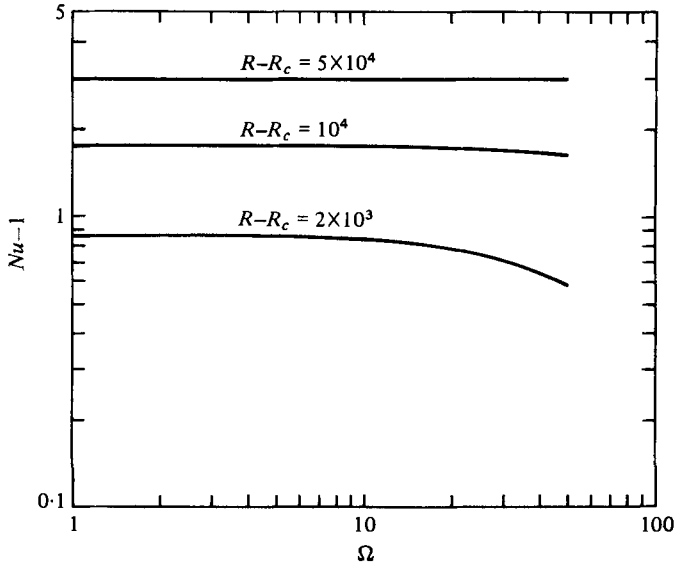

FIGURE 5. The Nusselt number shown as a function of Ω for different values of $R-R_c$ in the case $P = 7$, $\alpha = \alpha_c(\Omega)$.

wavelength of convection rolls as Somerville (1971) and Somerville & Lipps (1973) have suggested.

The Prandtl number dependence of the heat transport is shown in figure 7. It is clearly evident that the dependence is quite different in the regions $P < 1$ and $P > 1$. In some respects the heat transport varies in an opposite sense in rotating and in a non-rotating layer. While the heat transport in the non-rotating case increases monotonically with P for low values of R and exhibits a slight maximum at a Prandtl number of the order unity at high values of R, the opposite behaviour is shown for values of Ω larger than 30 in the range $P > 0{\cdot}1$. For sufficiently low Prandtl number,

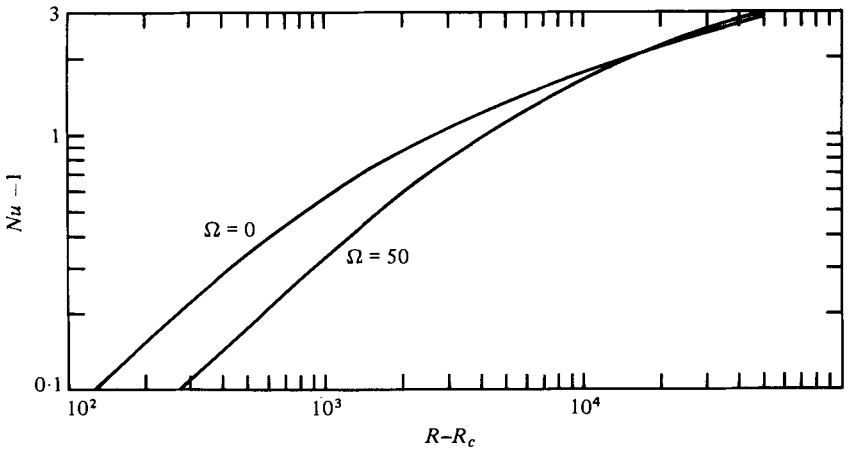

FIGURE 6. The Nusselt number as a function of Rayleigh number for two different values of Ω in the case $P = 7$, $\alpha = \alpha_c$.

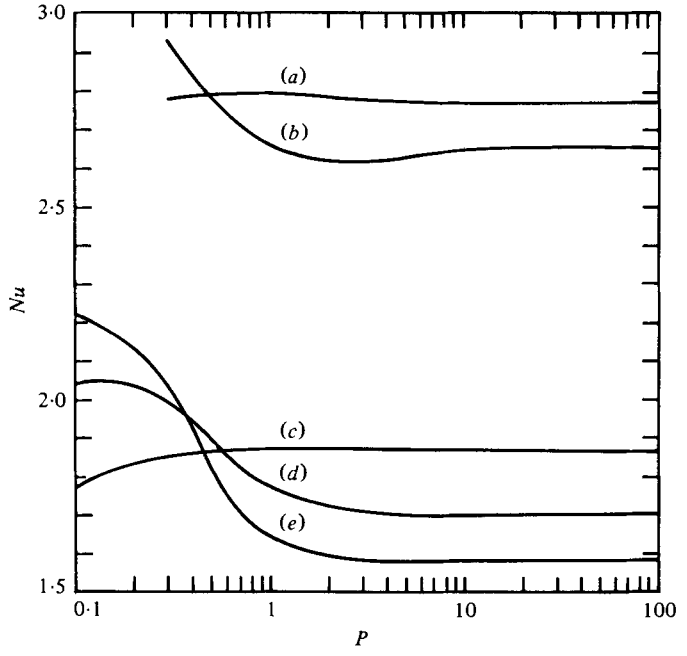

FIGURE 7. The Nusselt number as a function of the Prandtl number for different values of Ω and $R-R_c$. $R-R_c = 10^4$: (*a*) $\Omega = 0$; (*b*) $\Omega = 50$. $R-R_c = 2\times10^3$: (*c*) $\Omega = 0$; (*d*) $\Omega = 30$; (*e*) $\Omega = 50$.

the heat transport seems to decrease in every case, but the cost of computations for a converged solution increases strongly with decreasing P and the calculations have not been extended below $P = 0{\cdot}1$ for this reason.

The striking change of the dependence of the heat transport on $R-R_c$ for low Prandtl numbers is caused by the phenomenon of subcritical finite amplitude steady convection. We are using the word 'subcritical' here with respect to the onset of

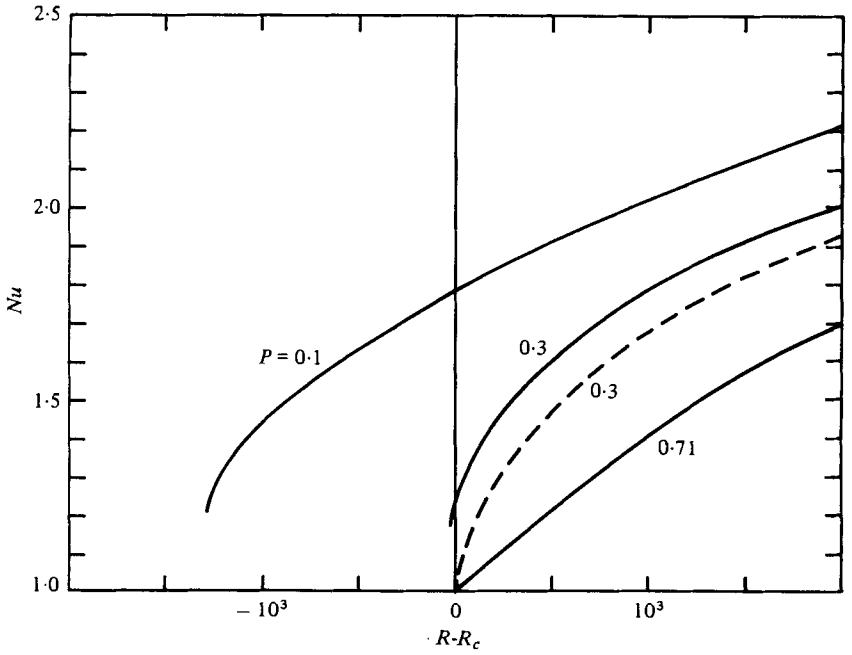

FIGURE 8. The Nusselt number as a function of $R - R_c$ in the case of low Prandtl number P for $\alpha = \alpha_c$. The solid and dashed curves correspond to $\Omega = 50$ and $\Omega = 100$, respectively.

steady convection modes. It is evident from figure 2 that the onset of oscillatory convection occurs at a critical value R_0 of the Rayleigh number, which is lower than R_c if the Prandtl number is sufficiently small. Within the parameter range where $R_0 < R_c$ finite amplitude steady convection does exist even for Rayleigh numbers less than R_0. This property was found by Veronis (1968) in the case of stress-free boundaries for an intermediate range of rotation parameter Ω. In the case of rigid boundaries, the occurrence of finite amplitude steady convection at Rayleigh numbers below those for the onset of oscillatory modes must be expected to be even more predominant since boundary conditions have a strongly inhibiting influence on oscillatory motions, while the critical Rayleigh number for steady convection is actually lower than for stress-free boundaries in the Ω-range of interest (Chandrasekhar 1961). Indeed, the case $P = 0{\cdot}1$, $\Omega = 50$ shown in figure 8 is an example of steady convection at Rayleigh numbers considerably below R_0. The results for $P = 0{\cdot}3$ and some others not shown in figure 8 indicate that the phenomenon of subcritical convection tends to disappear for high values of Ω, a property also found by Veronis (1968) in the stress-free case. As in the latter case, subcritical finite amplitude steady convection seems to occur only for the Prandtl numbers less than unity. The observation by Rossby (1969) of subcritical finite amplitude convection in a rotating layer of water can thus not be explained in terms of two-dimensional convection.

All results described so far have been obtained for convection rolls with the critical value α_c of the wavenumber corresponding to the minimum of the curves shown in figure 1. The variation of the heat transport with wavenumber is similar to that in a non-rotating layer if the Nusselt number is plotted as a function of $\alpha - \alpha_c$. Figure 9 shows the variation of the heat transport for $R = 10^4$ as an example. The stability

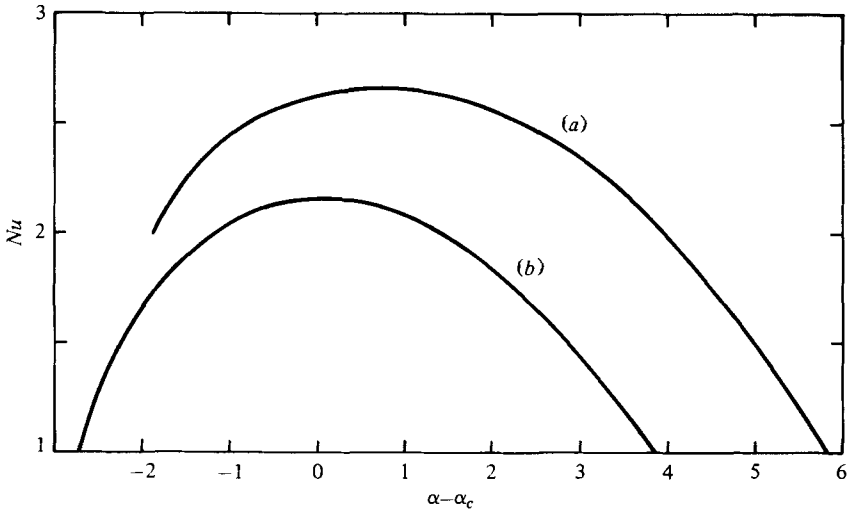

FIGURE 9. The Nusselt number as a function of the wavenumber for $\Omega = 0$ (a) and $\Omega = 50$ (b) in the case $R = 10^4$.

results discussed below confirm the impression that the effect of the varying wavenumber is similar to that in non-rotating case once the results have been expressed as a function of $\alpha - \alpha_c$.

4. Instabilities of steady convection rolls

4.1. *General discussion*

There are five known instability mechanisms that limit the stability domain of steady convection rolls in a non-rotating system. If the knot instability is counted as a mechanism distinct from the cross-roll instability, the number is six. From the physical point of view it is well justified to separate the two instabilities because of their different characteristic wavenumbers. But, from the mathematical point of view, the knot instability must be regarded as a modified form of the cross-roll instability. For a more detailed discussion the reader is referred to the latest paper on that subject by Busse & Clever (1979a). Because of the analytical dependence of the problem on the rotation parameter Ω, all instability mechanisms continue to operate in the case of steady convection rolls in a rotating system, at least if Ω is sufficiently small. Thus the discussion can be shortened by referring to CB and other earlier papers.

A new mechanism of instability occurring only in the case of a rotating layer has been discovered by Küppers & Lortz (1969). Mathematically, this mechanism is closely related to the skewed varicose instability in that it corresponds to finite values of both b and d in the representation (2.9) of the disturbance field. In contrast to the neutral disturbances of the skewed varicose type which correspond to the limit $d, b \to 0$ with finite ratio b/d, the Küppers–Lortz stability boundary corresponds to disturbances with finite values of b and d, such that $b^2 + (\alpha - d)^2$ assumes a value in the neighbourhood of α_c^2. Another difference between the two instability mechanisms besides the fact that the Küppers–Lortz instability occurs only for finite rotation rates is that the latter instability becomes independent of the Prandtl number P as

P tends to infinity, while the skewed varicose instability disappears for both high and low Prandtl numbers.

The skewed varicose and the Küppers–Lortz instabilities are, in general, obtained from disturbances for which the sum of the index λ and the index ν is an even integer. It is evident from the representation (2.9) that the same instabilities occur for disturbances with $\lambda+\nu =$ odd integers if d is replaced by $\alpha-d$. The numerical computations exhibit this invariance property within the accuracy expected for a finite value of the truncation parameter N. Actually, d could be replaced by $n\alpha+d$, where n is an arbitrary integer, without changing the stability problem, but the numerical results are closely similar only for $n = 0$ and $n = -1$ unless the truncation parameter N is increased beyond the values of 6 or 8 usually employed. The case of $\lambda+\nu =$ even appears to give the best approximation because d is usually smaller than $\alpha-d$.

Whenever possible, the calculations of the stability boundary for the onset of a certain instability have been continued into regions of the parameter space where steady convection rolls are unstable with respect to another instability and thus have been replaced by a three-dimensional convection flow. Although the mathematical results do not correspond to a physically realizable situation in this case, experience has shown that often the three-dimensional form of convection bccomes unstable in a similar fashion as has been theoretically predicted for the two-dimensional solution. But because of the mathematical similarity of the Küpper–Lortz and the skewed varicose instabilities, it is not always possible to distinguish them in regions where one of them has a finite positive growth rate. Since the wavenumbers d and b for the skewed varicose instability of maximum growth shift rapidly from vanishingly small to finite values past the stability boundary, the local maximum of σ as a function of b and d corresponding to the Küppers–Lortz instability may disappear on the shoulder of the maximum of the skewed varicose growth rate. This is actually happening to one of the branches of the Küpper–Lortz stability boundary shown in figure 10. Similar difficulties occur when the Küppers–Lortz stability boundary intersects the zig-zag stability boundary in figure 10. Although the strongest growing zig-zag disturbance corresponds to $d = 0$, disturbances with $d \neq 0$ also exhibit positive growth rates once the stability boundary has been crossed. Thus they can no longer be clearly separated in the computations from the Küppers–Lortz type disturbances.

4.2. *Stability boundaries*

Numerical solutions of the stability problem have been obtained primarily for the Prandtl numbers $P = 7$ and $P = 0{\cdot}71$, corresponding to water and air at room temperatures. Figure 10 displays the stability boundaries of steady convection rolls for $P = 7$, $\Omega = 10$. A comparison with the corresponding figure for $P = 7$, $\Omega = 0$ (Busse & Clever 1979*a*) shows that the Rayleigh number for the onset of the skewed varicose instability is slightly lowered by the effects of rotation. But at $\Omega = 10$ the Küppers–Lortz instability has just overtaken the skewed varicose instability in representing the boundary of the stability domain of rolls towards high Rayleigh numbers. A second branch of the Küppers–Lortz instability together with the zig-zag instability describes the boundary of the stability domain towards small wavenumbers. At $\Omega = 10$, the two branches cross each other, but at a somewhat larger value of Ω they join to form a single branch. This is evident from figure 11, which shows a much reduced stability domain for $\Omega = 15$. The determination of the value of Ω at which

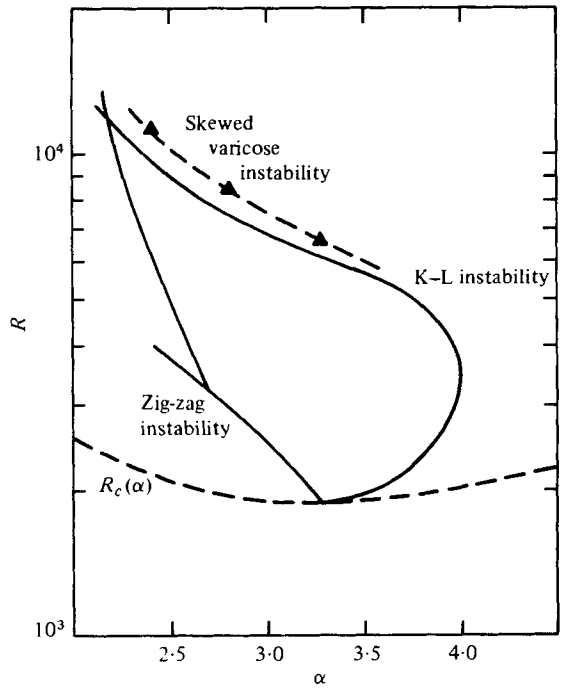

FIGURE 10. The stability region of steady convection rolls for $\Omega = 10$, $P = 7$. The lower dashed curve describes $R_c(\alpha)$.

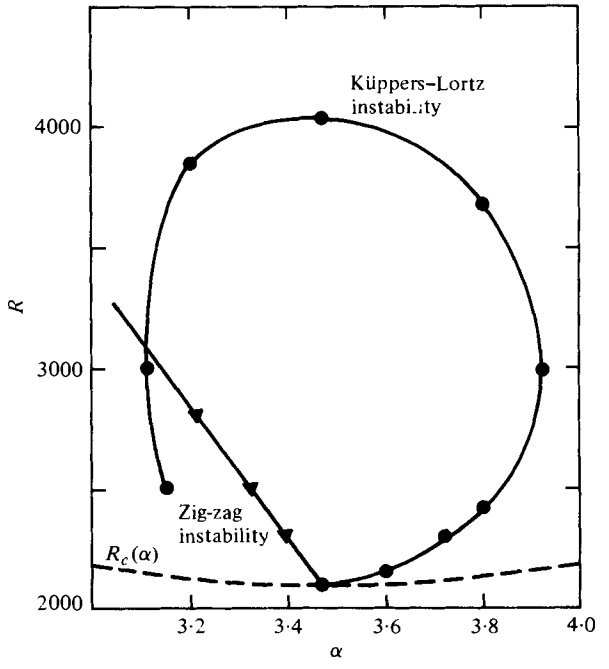

FIGURE 11. The same as figure 10 for $\Omega = 15$.

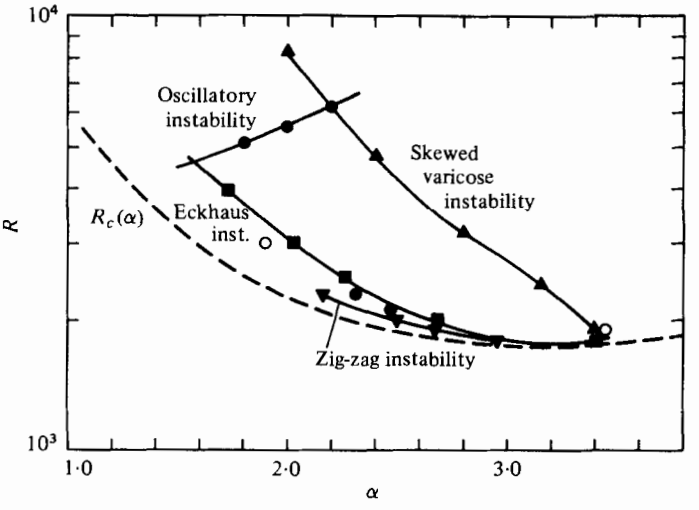

FIGURE 12. Stability region of steady convection rolls for $\Omega = 5$, $P = 0{\cdot}71$. The symbols ● and ○ give accurate and approximate positions, respectively, of the stability boundary for the Küppers–Lortz instability.

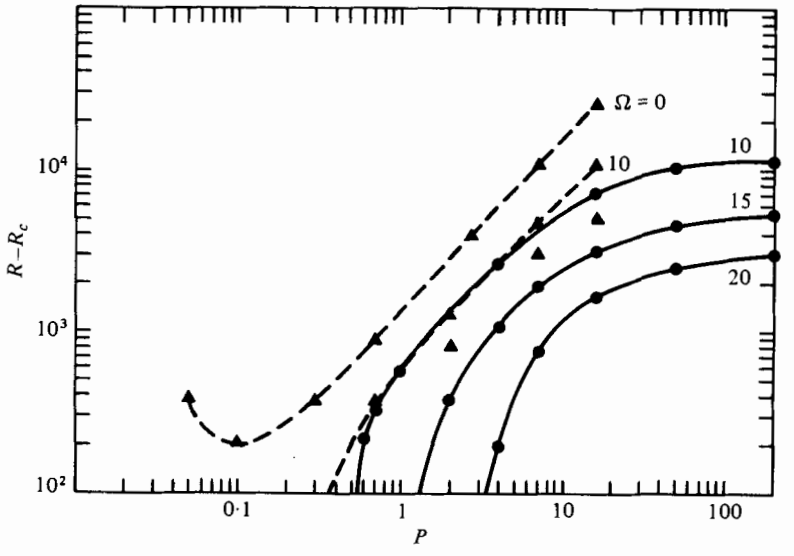

FIGURE 13. Stability boundaries for the skewed varicose (▲) and the Küppers–Lortz (●) instabilities in the case $\alpha = \alpha_c$ as a function of the Prandtl number for different values of Ω.

the two branches join requires expensive computations which have not been undertaken.

In the case $P = 0{\cdot}71$, the skewed varicose, the Eckhaus, and the oscillatory instability describe the stability boundary for $\Omega = 5$ in a similar way as they do for $\Omega = 0$ as shown in figure 12. At $\Omega = 10$ the Küppers–Lortz instability replaces the skewed varicose instability in determining the upper stability boundary. This is evident from figure 13, which indicates the critical Rayleigh number for the onset of both the skewed varicose and the Küppers–Lortz instability as a function of the

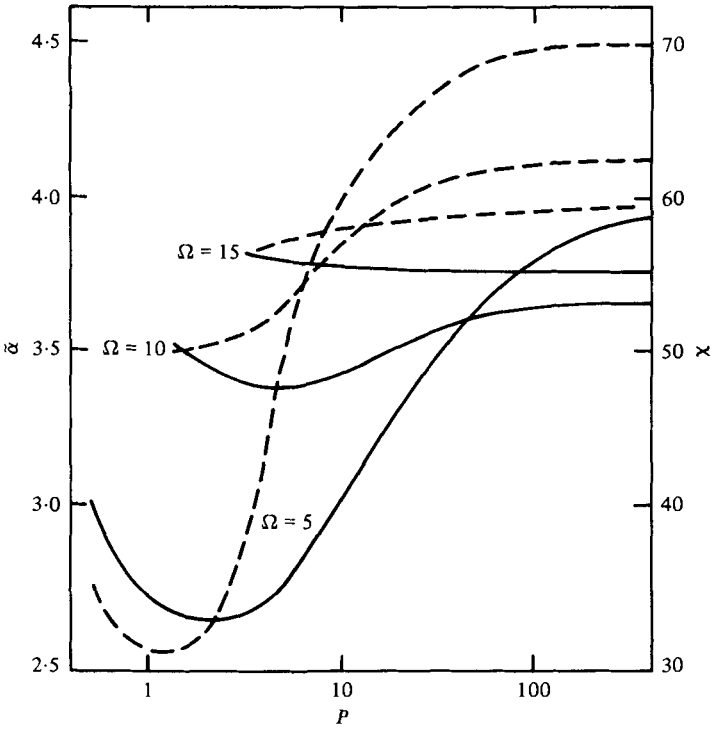

FIGURE 14. Wavenumber $\tilde{\alpha}$ (left ordinate, solid curves) and angle χ (right ordinate, dashed curves) of the Küppers–Lortz instability as a function of P for different values of Ω in the case $\alpha = \alpha_c$.

Prandtl number for various values of Ω. For $\Omega = 10$ the stability domain of steady rolls in the case $P = 0{\cdot}71$ has become so small that an exploration of the full stability boundary appeared to be of little interest. For slightly lower Prandtl numbers all steady two-dimensional solutions are unstable at $\Omega = 10$. At $\Omega = 15$ stable rolls can exist only for $P > 1$ and, for $\Omega \gtrsim 27$, rolls are unstable for all Prandtl numbers in agreement with the stability boundary $\Omega_c = 27{\cdot}39$ for $P = \infty$ determined by Küppers (1970, and personal communication) in the small amplitude limit.

The Küppers–Lortz type disturbances assume the form of parallel rolls enclosing the angle $\chi = \tan^{-1}[b/(\alpha - d)]$, with the steady rolls. This angle and the wavenumber $\tilde{\alpha} = [b^2 + (\alpha - d)^2]^{\frac{1}{2}}$ characterize the Küppers–Lortz instability and have been plotted for this reason in figure 14 as function of the Prandtl number. The three curves for both χ and α correspond to the three solid curves of figure 13. But the accuracy of the curves of figure 14 is much lower than in the other figures, since special computations for the accurate determination of b and d have not been made and either wavenumber may differ from its exact value by several per cent. Since the growth rate assumes a maximum at the critical values of b and d, the accuracy of the computations of the stability boundary is not affected in first order. Figure 14 indicates that the wavenumber $\tilde{\alpha}$ differs little from the value α_c of the steady solution. For low values of P and Ω the variations of $\tilde{\alpha}$ become more pronounced, a behaviour which is also shown by the angle χ. As Ω increases, χ approaches a value in the neighbourhood of 58°,

which is the angle found by Küppers & Lortz (1969) in their analysis for stress-free boundaries and $P = \infty$.

Figure 14 shows the variations of $\tilde{\alpha}$ and χ only in the case when $\alpha = \alpha_c$. For other values of α the results for $\tilde{\alpha}$ and χ are not much different, except that χ approaches angles near 90° at the lower part of the Küppers–Lortz stability boundary for $\alpha > \alpha_c$ shown in figure 10. The value of $\tilde{\alpha}$ stays close to α_c throughout the stability boundary.

5. Discussion

The analysis of this paper has confirmed and extended the result of Küppers & Lortz (1969) that all steady small amplitude solutions are unstable when the rotation rate is sufficiently large. This poses a problem which has implications for the general theory of hydrodynamic instability and turbulence. Since oscillatory forms of convection do not exist for $P > 1$, the puzzling question arises of which form of convection is physically realized. An answer to this question can be obtained when the full time-dependent three-dimensional problem posed by equations (2.1) is solved. Using a three-mode approximation in the limit of small amplitudes, time-dependent solutions have been obtained in a recent paper (Busse & Clever 1978*b*). Unpublished results with up to 60 modes describing the horizontal pattern of convection have led to essentially the same results.

Starting with a two-dimensional solution of the stationary problem and a set of small amplitude disturbance fields, the Küppers–Lortz instability develops as predicted by the linear theory. In the particular case considered by Busse & Clever (1979*b*) a disturbance in the form of rolls enclosing an angle of 60° with the given rolls grows and finally replaces the original roll solution. At this point a new disturbance in the form of rolls enclosing an angle of 120° with the direction of the original rolls starts to grow. Thus the process of instability is repeated in a cyclic fashion. The results show the unrealistic feature that the time from one cycle to the next increases without bound since the disturbances start growing from decreasing amplitudes. To represent the role of experimental noise in providing a constant level for the initial amplitudes of disturbances, a lower bound for the amplitudes of modes was introduced in a second series of computations. This leads to periodic solutions in the form of rolls that change their direction by 60° after each third of the full cycle. Consideration of the statistical nature of the experimental noise will lead to quasi-periodic solutions in the statistical mean. Convection in a rotating layer thus represents a particularly simple realization of a turbulent fluid system in that statistical properties govern the time dependence of the convection flow at all times.

The above picture is basically confirmed by the experimental observations being carried out presently at UCLA (Ph.D. research project of K. E. Heikes). Earlier experimental observations by Rossby (1969) and Krishnamurti (1971) were done at Rayleigh numbers well above the critical value for onset of convection and indicated a transition from two-dimensional rolls to a three-dimensional cellular pattern of convection. Thus there appears to exist another stability boundary which describes the minimum Rayleigh number for which a cellular form of convection can be realized. Because the Rayleigh numbers of interest correspond to a few times the critical value, three-dimensional numerical computations appear to be feasible, but a systematic approach to the problem has not yet been undertaken. Some examples of

three-dimensional convection in a rotating system have been computed by Somerville & Lipps (1973) using a finite difference scheme. They were able to explain the non-monotone dependence of the heat transport on the rotation rate owing to the change of the wavelength of convection rolls, and they demonstrated that a three-dimensional cellular form of convection is preferred at high Rayleigh numbers. A further numerical exploration of three-dimensional convection in a rotating system would be of great interest in order to confirm the hypothesized additional stability boundary and to gain a better understanding of the nature of the cellular form of convection.

Because of the sparsity of quantitative experimental results, a comparison between theoretical predictions and observations is not attempted in this paper. The only published measurements of the parameters for the onset of the Küppers–Lortz instability are those by Krishnamurti (1971). At Rayleigh numbers of 4–7 times the critical value, the theoretical results agree with the experimental data, but, at lower Rayleigh numbers, Krishnamurti's graph suggests that the onset of the instability becomes independent of the Rayleigh number, while the results displayed in figure 9, together with those of Küppers (1970), indicate a continuing increase of the critical value of Ω with decreasing R. In the new experimental study of K. E. Heikes, mentioned above, this discrepancy will be investigated in detail.

The financial support of the NSF Atmospheric Sciences Section is gratefully acknowledged.

REFERENCES

Busse, F. H. 1967*a* The stability of finite amplitude cellular convection and its relation to an extremum principle. *J. Fluid Mech.* **30**, 625–649.

Busse, F. H. 1967*b* On the stability of two-dimensional convection in a layer heated from below. *J. Math. Phys.* **46**, 140–150.

Busse, F. H. 1972 The oscillatory instability of convection rolls in a low Prandtl number fluid. *J. Fluid Mech.* **52**, 97–112.

Busse, F. H. & Clever, R. M. 1979*a* Instabilities of convection rolls in a fluid of moderate Prandtl number. *J. Fluid Mech.* **91**, 319–335.

Busse, F. H. & Clever, R. M. 1979*b* Nonstationary convection in a rotating system. In *Recent Developments in Theoretical and Experimental Fluid Mechanics – Compressible and Incompressible Flows* (ed. U. Müller, K. G. Roesner & B. Schmidt), pp. **376–385**. Springer.

Busse, F. H. & Whitehead, J. A. 1971 Instabilities of convection rolls in a high Prandtl number fluid. *J. Fluid Mech.* **47**, 305–320.

Busse, F. H. & Whitehead, J. A. 1974 Oscillatory and collective instabilities in large Prandtl number convection. *J. Fluid Mech.* **66**, 67–79.

Chandrasekhar, S. 1961 *Hydrodynamic and Hydromagnetic Stability*. Oxford: Clarendon Press.

Clever, R. M. & Busse, F. H. 1974 Transition to time dependent convection. *J. Fluid Mech.* **65**, 625–645.

Clever, R. M. & Busse, F. H. 1977 Instabilities of longitudinal convection rolls in an inclined layer. *J. Fluid Mech.* **81**, 107–127.

Clever, R. M. & Busse, F. H. 1978 Large wavelength convection rolls in low Prandtl number fluids. *Z. angew. Math. Phys.* **29**, 711–714.

Hart, J. E. 1971 Transition to a wavy vortex regime in convective flow between inclined plates. *J. Fluid Mech.* **48**, 265–271.

Koschmieder, E. L. 1967 On convection on a uniformly heated rotating plane. *Beitr. Phys. Atmosph.* **40**, 215–225.

KRISHNAMURTI, R. 1971 On the transition to turbulent convection. *8th Symp. on Naval Hydrodyn., rep.* ARC-179, pp. 289–310. Office of Naval Research.

KÜPPERS, G. 1970 The stability of steady finite amplitude convection in a rotating fluid layer. *Phys. Lett.* A **32**, 7–8.

KÜPPERS, G. & LORTZ, D. 1969 Transition from laminar convection to thermal turbulence in a rotating fluid layer. *J. Fluid Mech.* **35**, 609–620.

ROSSBY, H. T. 1969 A study of Bénard convection with and without rotation. *J. Fluid Mech.* **36**, 309–335.

SCHLÜTER, A., LORTZ, D. & BUSSE, F. H. 1965 On the stability of steady finite amplitude convection. *J. Fluid Mech.* **23**, 129–144.

SOMERVILLE, R. C. J. 1971 Bénard convection in a rotating fluid. *Geophys. Fluid Dyn.* **2**, 247–262.

SOMERVILLE, R. C. J. & LIPPS, F. B. 1973 A numerical study in three space dimensions of Bénard convection in a rotating fluid. *J. Atmos. Sci.* **30**, 590–596.

VERONIS, G. 1966 Motions at subcritical values of the Rayleigh number in a rotating fluid. *J. Fluid Mech.* **24**, 545–554.

VERONIS, G. 1968 Large-amplitude Bénard convection in a rotating fluid. *J. Fluid Mech.* **31**, 113–139.